ESTIMATING THE NUMBER OF ACTIVE DEVICES WITHIN A FIXED AREA

USING WI-FI MONITORING

A Thesis

by

HAI LI

Submitted to the Office of Graduate and Professional Studies of
Texas A&M University
in partial fulfillment of the requirements for the degree of

MASTER OF SCIENCE

Chair of Committee,   Jean-Francois Chamberland
Committee Members,   Gregory H. Huff
                                      Anxiao Jiang
                                      Tie Liu
Head of Department,   Jose Silva-Martinez

December 2016

Major Subject: Electrical Engineering

ABSTRACT

In various situations, there is a need to estimate the number of active Wi-Fi enabled devices, like smartphones, within a specific area. This thesis offers one possible approach to accomplish this task. It focuses on estimating the number of devices in a certain area based on monitoring and processing Wi-Fi metadata, which includes a received signal strength indicator. To accomplish this goal, four sensing devices are placed at the corners of a rect-angular area. These sensing devices observe and record local data traffic, along with the received signal strength associated with each packet. For each sensing device, two types of frontends are considered, namely directional and isotropic antennas. Each sensing device retrieves the received signal strength indicators and the media access control addresses from the 802.11 frames packets transmitted by nearby active wireless devices. The es-timator takes the received signal strength indicators as input and infers the number of active Wi-Fi devices inside the area of interest. Two algorithms, bayesian and maximum-likelihood, are employed for estimation purposes. Overall performance is used to compare and contrast the systems implemented with directional antennas and isotropic antennas, re-spectively. Theoretical and experimental results both hint at performance improvements when using directional antennas, when compared to standard isotropic antennas.

DEDICATION

This dissertation work is dedicated to my father, my mother, my friends for their support

throughout the process.

ACKNOWLEDGMENTS

NOMENCLATURE

RSSI   Received Signal Strength Indicator

MAC   Media Access Control

NUC   Intel's Next Unit of Computing device

BMSE   Bayesian Mean Square Error

MSE   Mean Square Error

TABLE OF CONTENTS

Page

LIST OF FIGURES

LIST OF TABLES

1. INTRODUCTION

Occupancy estimation refers to the problem to estimate the number of people inside a certain area. This topic has attracted lots of interests for years due to its importance. There are several potential applications that can benefit from occupancy estimation. In smart building automation systems, using knowledge of the level of occupancy, it is possible to optimize the energy cost over the control of temperature and ventilation. This can result in a large amount of energy saving [1, 2]. In navigation systems, providing road occupancy traffic information will allow users to find out the best route to the destination. In [3], the author proposed a road monitoring system that encompass UMTS and GPRS data collection. Under an emergency circumstance, a proper occupancy estimation may help the government guide the evacuation of crowds.

In recent years, the number of Wi-Fi access points and the number of Wi-Fi client devices have been increasing dramatically. This growth in Wi-Fi infrastructure leads to large amounts of data being transmitted over wireless networks. Cisco Systems predicts in their Visual Network Index that 55 percent of total mobile data traffic will be offloaded onto fixed networks through Wi-Fi access points and femtocells by 2020 [4]. This means Wi-Fi is increasingly becoming a prime data source since Wi-Fi signals can tell us about our environment. A lot of attention is drawn into this area, with topics such as self-localization, source localization and occupancy estimation [5, 6].

At the same time, we have witnessed the rapid development of mobile technology which is fuelled by a large amount of smartphone users. Smartphone supports real-time communication and information access, with an advanced mobile operating system that combines features of a personal computer and other features useful for mobile use. Smartphones are influencing human activity significantly. The global smartphone penetration

rate has grown fast over past years. According to eMarketer's prediction in [7], smart-phone user penetration as percentage of total global population will be 34.64 percent by 2019. In the U.S., 197.4 million people owned smartphones (79.3 percent mobile market penetration) during the three months ending in December 2015 according to comScore's report [8]. This rapid development demands an improved manufacturing process. As the result, mass production involved in smartphone technology have decreased the cost of smartphone components. This fact makes smartphones price-friendly to users. Notably smartphone operation systems also play important roles in mobile devices. For instance, Android system provides the manufacturer a tool to produce multi-platform applications for smartphones. This makes the development procedure cheaper and it gets devices in the hands of more people. Overall, the continuous growth in mobile technology attracts more attention into this field.

1.1 The Wireless Environment

In this work, we are interested in the occupancy estimation based on Wi-Fi activity of the users. A good understanding of the wireless channel is key to analyze communication systems. With this in mind, we will discuss important concepts in channel modeling like path loss, shadow fading and multipath propagation. Path loss refers to the attenuation in the transmitted signal while propagating from the transmitter (Tx) to the receiver (Rx). Received signal power is a function of the distance between Tx and Rx. The simplest path loss model is used for unobstructed line-of-sight (LOS) signal path in free space propagation. Under this model, the received signal is given by

$$P_R = P_T G_T G_R \frac{\lambda^2}{4\pi d^2} \tag{1.1}$$

where P_T is the transmitted power, G_T and G_R are the transmit and receive antenna gains, respectively, λ is the transmitted carrier wavelength, and d is the distance between

2

Tx and Rx. Thus, the received power falls off proportional to the ratio of wavelength over distance squared. This also establishes the relation between path loss and wave length: a shorter wave length implies a higher path loss. Though simple, the free space path loss model is of limited value in real environments. Therefore, we need to take more factors into consideration.

In the previous path loss model, we assume the path loss to be constant if the distance is given. However in reality, the presence of obstacles like buildings and trees between transmitter and receiver may bring random variations in path loss. This effect is due to changes in scattering, reflecting and diffracting surfaces in the propagation environment and it is called shadowing [9]. Considering shadowing, the received signal power becomes

$$P_R = P_T G_T G_R S \tag{1.2}$$

where P_L and S correspond to the path loss and the shadow fading factor,respectively. Above, S is a random variable. Experiment results show that a log-normal distribution function provides a good match to the empirical probability density function (PDF) of the shadow fading component [10]. Therefore, the pdf of S can be approximated as the pdf of a Gaussian random variable when S is expressed in the logarithmic (dB) domain:

$$f_{S_s}(s) = \frac{1}{\sqrt{2\pi}\sigma_{\mathrm{s}}} \exp\left(-\frac{s^2}{2\sigma_{\mathrm{s}}^2}\right) \tag{1.3}$$

where σ_{s} is the standard deviation of shadowing. Typically σ_{s} is between 5-10 dB.

Multipath fading occurs as a result of signal reflections, diffractions, and/or scattering on objects before reaching the destination. Multiple copies of the signal may arrive at different phases. Multipath fading may also cause inter-symbol interference. Compared with shadowing fading, multipath fading is a short-term factor that generally causes smaller effects to the signal power. Therefore, the multipath fading is also called small-scale fad-

ing. Some model such as Rayleigh fading and Ricean fading can be used for multipath fading [9]. Rayleigh fading is a reasonable model when there are many objects in the environment that scatter the radio signal before it arrives at the receiver. However, when a LOS exists or a strong reflected path, termed specular component, also arrives at the receiver, the fading is more appropriately modeled by a Rician distribution [11]. Several different models such as Okumura, Hata, Walfish-Ikegami have been proposed to model different environments like urban, rural and indoor areas [11].

Current literature on occupancy estimation is largely based on either images or RF signals. Approaches based on cameras use captured images to estimate the number of people in a crowded scene [12, 13, 14]. Still, in such camera-based approaches, estimation accuracy can be affected by many factors such as brightness and image resolution. In addition, camera-based approaches typically lead to high deployment cost, which makes it inconvenient to deploy in reality. On the other hand, occupancy estimation based on RF signals is more promising. This category encompasses several methods. Passive infrared sensor is one of the common technologies used in the past few years. In [15], the authors propose an occupancy estimation system which is able to adjust with movement of the people inside the building. They shows that about 5% more energy can be saved by using smart occupancy sensor as compared to non-adapting fixed time-delay sensors. In [16], an indoor occupancy estimation using ultrasonic chirps is proposed. The author shows that the average error in percentage to the maximum capacity of the room is around 5%. Yet, this option is an active sensing system; if multiple transducers are placed in the same room, they can interfere with one another.

Other methods involved Bluetooth [17] and Wi-Fi [18]. However, the short transmission range limits the performance of Bluetooth-based methods. A research compared Wi-Fi and Bluetooth approaches [19]. In their work, the authors stipulate that Wi-Fi has advantage over Bluetooth in monitoring people, due to shorter discovery time and higher

detection rates. According to their results, more than 90% of scanned unique MAC addresses in all places are Wi-Fi addresses; the popularity of using Wi-Fi devices is therefore significantly higher than that of Bluetooth devices, which means occupancy estimation using Wi-Fi is much more convenient in practice. In [20], the author proposes FCC, a device-Free Crowd Counting approach based on channel state information measurements. In [21], the author develops a new approach for estimating the total number of people walking in an area with only Wi-Fi power measurements between a pair of stationary transmitter/receiver antennas. In this latter case, they do not need the measurement of channel state information.

In this thesis, we are interested in estimating the number of active devices in a fixed area using Wi-Fi metadata. Modern mobile devices equipped with Wi-Fi modules transmit Wi-Fi messages periodically. Therefore, this provides a means to estimate occupancy by passively listening to Wi-Fi packets. More specifically, by deploying Wi-Fi monitoring devices in an area of interest, it is possible to detect Wi-Fi transmissions. Each acquired Wi-Fi packet contains a unique MAC address. This information can be augmented by the received signal strength indicator (RSSI) of the captured signal. In the current context, the MAC address serves as a device identifier, whereas the RSSI provides partial information about the physical distance between the transmitter and the monitoring device. This information is helpful in inferring the device location status. The existence of `pcap`, an application programming interface for capturing network traffic, and wireshark, a network protocol analyzer, makes the Wi-Fi traffic analysis straightforward.

In the research, we focus on occupancy estimation based on Wi-Fi packets and we analyze the benefits associated with using directional antennas. On the one hand, we are going to introduce two stochastic estimation schemes. One is a Bayes estimation scheme and the other is a maximum likelihood scheme. On the other hand, we will investigate the benefits of using directional antennas in monitoring devices. Because the radiation pattern of an

5

antenna will influence the RF propagation, it is naturally to think of the potential impacts it brings to use directional antennas. We employ numerical simulations to compare the performance of different schemes corresponding to sensing devices with directional antennas and isotropic antennas. In simulations, we assume that four sensing devices are located in the four corners of a rectangular target area. The training RSSI values are assumed to obey free-space path loss model as well. Our results indicate that, when directional antennas are employed, the error rate decreases considerably. In addition, our findings are further supported through outdoor experimentation. The testbed is implemented in a line-of-sight environment, with four sensing devices deployed at the corners of the area of interest.

The remainder of this thesis is organized as follows. In Section 2, we explain our problem formulation and develop a probability model. In Section 3, we propose two algorithms for occupancy estimation. These schemes are evaluated through numerical simulations in Section 4. We then discuss experimental results, along with description of experiment setup in Section 5. Finally, we offer concluding remarks in Section 6.

2. SYSTEM MODEL AND PROBLEM FORMULATION

Wi-Fi based occupancy estimation is attractive because it only require simple sensing devices. Meanwhile, it can benefit from local Wi-Fi network and the high penetration rate of smartphones. The existence of tools like `pcap` and wireshark makes monitoring Wi-Fi environments a straightforward task. In this thesis, we extract the RSSI and MAC address for the purpose of occupancy estimation. As discussed above, the RSSI is related to the distance between the Rx and Tx. Thus, we can estimate the location information based on RSSI values. Still, RSSI does not depend only on distance; some other factors like noise and fading can also influence it. As such, a proper wireless channel model is needed to take care of this situation.

2.1 Wireless Channel Model

A common wireless environment can be express as

$$r(t) = g(d)s(t) + w(t),$$

where $r(t)$ represents the received signal; the function $g(d)$ is the power gain which is related to several factors including the mean path loss, shadow fading and antenna gain; $s(t)$ denotes the sent signal; and $w(t)$ is noise. Herein, we adopt the log-normal channel model. So, the expected received power for a given distance between transmitter and receiver can be expressed as

$$P_d[\text{dBm}] = A + B \log_{10}(d) + L_s + G_a, \tag{2.1}$$

where A is a combination of the transmitted signal power and average path loss and B represents the path loss coefficient. Component L_s is a Gaussian random variable that

captures shadowing. Finally, G_a is the antenna gain. We note that the mean of L_s can be added in A; thus, we assume L_s is a zero mean random variable, $L_s \sim \mathcal{N}(0, \sigma_s^2)$. Parameter σ_s is the variance of the shadowing component. In the logarithmic domain, the probability density function of L_s can be written as

$$f_{L_s}(\ell) = \frac{1}{\sqrt{2\pi}\sigma_s} \exp\left(-\frac{\ell^2}{2\sigma_s^2}\right).$$

Its variance can be estimated using the sampled data. An unbiased estimator for the variance is given by [22]

$$\sigma_s^2 = \frac{1}{N-1} \sum_1^N (l_k - \mu_s)^2,$$

where N is the sample size, l_k forms the data set, and points are expressed in the logarithmic domain [23, 24].

In a practical setting, we need to estimate the wireless channel parameters A and B. To do so, we use the method of least squares, which minimizes the sum of the squares of the offsets. Consider the linear least squares problem given by

$$f(x, \beta) = \sum_{j=1}^m \beta_j \phi_j(x),$$

where ϕ_j is a function of x and β is the parameter vector to be estimated. Letting matrix M be defined as

$$M_{ij} = \frac{\partial f(x_i, \boldsymbol{\beta})}{\partial \beta_j} = \phi_j(x_i),$$

the least squares estimate for β becomes

$$\hat{\boldsymbol{\beta}} = (M^T M)^{-1} M^T \mathbf{y}.$$

For the least square problem defined in Section 2.1, we get

$$\underset{a,b}{\mathrm{argmin}} \left\| \underbrace{\begin{bmatrix} \vdots \\ p_{ij} - G_i(\phi_{ij}) \\ \vdots \end{bmatrix}}_{\mathbf{y}} - \underbrace{\begin{bmatrix} \vdots & \vdots \\ 1 & \log_{10}(d_{ij}) \\ \vdots & \vdots \end{bmatrix}}_{M} \begin{bmatrix} a \\ b \end{bmatrix} \right\|^2 .$$

Then, the estimator of A and B is given as

$$\begin{bmatrix} A \\ B \end{bmatrix} = \left(M^{\mathrm{t}}M\right)^{-1} M^{\mathrm{t}}\mathbf{y}.$$

The variance of L_s, the shadow fading component, is computed by normalizing the residual error

$$\sigma_{\mathrm{s}}^2 = \frac{1}{N-1}\mathbf{y}^T(I - M(M^TM)^{-1}M^T)\mathbf{y}.$$

2.2   Problem Formulation

Consider a scenario where several wireless devices are randomly positioned nearby an area of interest. To simplify the problem, we assume the area to be rectangular shape. Four RF monitoring devices are located at the corners of this region. Each monitoring device has information concerning its own location and orientation. The radiation pattern of the antenna attached to each monitoring device is known as well. In our system model, all of the monitoring devices are connected to the Internet and send the captured data to a process center for inference. Several wireless clients carried by users are randomly located near this area, they can be inside or outside the area of interest. The wireless clients transmit data packets periodically and, consequently, they can be easily detected by the monitoring devices. Since each wireless client has a unique MAC address, the packets transmitted

9
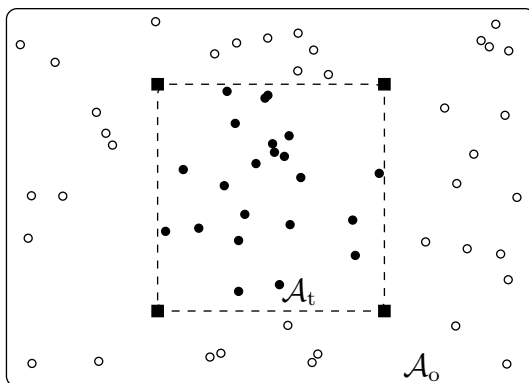
Figure 2.1: The periphery of the target area is delineated by the dashed line. The squares at the corners of the target area denote the locations of the monitoring devices, each equipped with a directional antenna. Clients within the zone of interest are in black, whereas outside agents appear in white. The objective is to estimate the occupancy within target area.

from different clients can be distinguished. Throughout, we use $\mathcal{A}_t$ to represent the target area and $\mathcal{A}_o$ to represent its complement. A notional diagram of the framework is shown in Fig. 2.1.

In this thesis, we assume the wireless clients are quasi-static and each client is equipped with an isotropic antenna. Thus, the orientation of the wireless clients does not matter. For convenience, we use a single vector to denote the locations of the wireless clients:

$$\underline{\mathbf{U}} = (\mathbf{U}_1, \dots, \mathbf{U}_{n_a}), \tag{2.2}$$

where n_a is the number of the detected clients. We also assume that the signal captured by a monitoring device comes from a line-of-sight path. Therefore, signal strength subscribes to a free-space transmission model. The received signal strength from client j to sensing device i can be expressed using the log-normal channel model

$$P_{ij}[\text{dBm}] = A + B \log_{10}(d_{ij}) + L_{ij} + G_i(\phi_{ij}), \tag{2.3}$$

where A and B are the mean decay parameters, d_{ij} is the Euclidean distance between the client j and sensing device i. This distance is equal to

$$d_{ij} = d(\mathbf{s}_i, \mathbf{u}_j) = \sqrt{(u_{1j} - s_{1i})^2 + (u_{2j} - s_{2i})^2}.$$

Variable L_{ij} represent shadow fading and parameter $G_i(\cdot)$ is the antenna gain function of the sensing device. Parameter ϕ_{ij} denotes the angle of the signal transmission direction, which can be expressed as

$$\phi_{ij} = \angle(\mathbf{s}_i, \mathbf{u}_j) = \text{atan2}(u_{2j} - s_{2i}, u_{1j} - s_{1i}).$$

The shadow fading components $\{L_{ij}\}$ are assumed to be independent and identically distributed log-normal random variables. In the logarithmic domain, the corresponding probability density function becomes

$$f_{L_{ij}}(\ell) = \frac{1}{\sqrt{2\pi}\sigma_{\text{s}}} \exp\left(-\frac{\ell^2}{2\sigma_{\text{s}}^2}\right), \tag{2.4}$$

where σ_{s} is the standard deviation of shadowing.

The observed information from the four sensing devices form a power matrix $\underline{\mathbf{P}} = (\mathbf{P}_1, \ldots, \mathbf{P}_{n_{\text{a}}})$. The vector element $\mathbf{P}_j = (P_{1j}, P_{2j}, P_{3j}, P_{4j})$ contains the signal strength of the wireless client j detected by four sensing devices. We assume that the number and locations of the wireless clients located inside the area of interest form a Poisson point process with intensity λ_{t}. Therefore, the probability that r_t wireless clients lie inside the target area is equal to

$$\Pr(R_{\text{t}} = r_{\text{t}}) = \frac{(\lambda_{\text{t}} A_{\text{t}})^{r_{\text{t}}}}{r_{\text{t}}!} e^{-A_{\text{t}}\lambda_{\text{t}}} \quad r_{\text{t}} = 0, 1, \ldots$$

where R_{t} is the number of clients inside and A_{t} is the area of the target region. Sim-

ilarly, we can write the probability that r_o wireless clients are located outside the target area as

$$\Pr(R_o = r_o) = \frac{(\lambda_o A_o)^{r_o}}{r_o!} e^{-A_o \lambda_o} \quad r_o = 0, 1, \ldots$$

where R_o is the number of clients outside, A_o is the area of the complement of target region, and λ_o is a Poisson intensity parameter. The inference task is to estimate occupancy based on the power matrix data set $\underline{\mathbf{P}}$, which is collected by the sensing devices.

3. ESTIMATION SCHEMES

In this section, we introduce the two estimation schemes employed in this thesis. A Bayes estimation scheme and a maximum likelihood estimation algorithm are considered and they are applied under different scenarios. If the estimation process is applied repetitively over time, then acquired data can be employed to gain accurate estimates for λ_t and λ_o. In other words, λ_t and λ_o are considered known. In such scenarios, Bayes estimation is employed. On the other hand, if the occupancy estimation is applied to an area of interest once, then we can use a classic framework such as maximum likelihood estimation.

3.1 Bayes Estimation

In the Bayes estimation scheme, we assume the Poisson intensity parameters λ_t and λ_o are known. Our objective is to estimate the number of clients inside the target area based on observed data $\underline{\mathbf{P}}$. First, we need to get the posterior distribution of R_t, given $\underline{\mathbf{P}}$,

$$
\begin{aligned}
\Pr\left(R_t = r_t | \underline{\mathbf{P}} = \underline{\mathbf{p}}\right) &= \int_{\{\underline{\mathbf{u}}: R_t(\underline{\mathbf{u}})=r_t, R_o(\underline{\mathbf{u}})=r_o\}} f_{\underline{\mathbf{U}}|\underline{\mathbf{P}}}\left(\underline{\mathbf{u}}|\underline{\mathbf{p}}\right) d\underline{\mathbf{u}} \\
&= \int_{\{\underline{\mathbf{u}}: R_t(\underline{\mathbf{u}})=r_t, R_o(\underline{\mathbf{u}})=r_o\}} \frac{f_{\underline{\mathbf{P}}|\underline{\mathbf{U}}}\left(\underline{\mathbf{p}}|\underline{\mathbf{u}}\right) f_{\underline{\mathbf{U}}}(\underline{\mathbf{u}})}{f_{\underline{\mathbf{P}}}\left(\underline{\mathbf{p}}\right)} d\underline{\mathbf{u}}
\end{aligned}
\tag{3.1}
$$

where $\underline{\mathbf{U}}$ is the location vector containing the random positions of the wireless clients. The location vector includes lots of information. For example, the size of $\underline{\mathbf{U}}$ is the number of active wireless clients. According to the location vector, we can get the number of wireless clients inside or outside the target area. Thus, R_t and R_o can be viewed as functions of $\underline{\mathbf{U}}$. Because the outside and inside Poisson processes are independent, the distribution of $\underline{\mathbf{U}}$ can be written as

$$f_{\underline{U}}(\underline{u}) = \frac{1}{A_t^{R_t(\underline{u})}} \frac{(\lambda_t A_t)^{R_t(\underline{u})}}{(R_t(\underline{u}))!} e^{-A_t \lambda_t} \frac{1}{A_o^{R_o(\underline{u})}} \frac{(\lambda_o A_o)^{R_o(\underline{u})}}{(R_o(\underline{u}))!} e^{-A_o \lambda_o}$$

$$= \frac{\lambda_t^{R_t(\underline{u})}}{(R_t(\underline{u}))!} \frac{\lambda_o^{R_o(\underline{u})}}{(R_o(\underline{u}))!} e^{-A_t \lambda_t - A_o \lambda_o}. \tag{3.2}$$

For a wireless client j, the distribution of the received power vector $\mathbf{P}_j$ given a specific location $\mathbf{u}_j$ is equal to

$$f_{\mathbf{P}_j | \mathbf{U}_j}(\mathbf{p}_j | \mathbf{u}_j) = \prod_{i=1}^{n_s} f_{L_{ij}}(p_{ij} - A - B \log_{10}(d_{ij}) - G_i(\phi_{ij}))$$

$$= \frac{1}{(2\pi\sigma_s^2)^{\frac{n_s}{2}}} \prod_{i=1}^{n_s} e^{-\frac{(p_{ij} - A - B \log_{10}(d_{ij}) - G_i(\phi_{ij}))^2}{2\sigma_s^2}} \tag{3.3}$$

$$= (2\pi\sigma_s^2)^{-\frac{n_s}{2}} e^{-\frac{\sum_{i=1}^{n_s}(p_{ij} - A - B \log_{10}(d_{ij}) - G_i(\phi_{ij}))^2}{2\sigma_s^2}}.$$

The conditional distribution of $\underline{P}$ given $\underline{U} = \underline{u}$, is then

$$f_{\underline{P}|\underline{U}}\left(\underline{p}|\underline{u}\right) = \prod_{j=1}^{n_a} f_{\mathbf{P}_j|\mathbf{U}_j}(\mathbf{p}_j|\mathbf{u}_j). \tag{3.4}$$

With the conditional distribution of $\underline{P}$ given $\underline{U} = \underline{u}$ and the distribution of $\underline{U}$, we can compute the marginal distribution of $\underline{P}$,

$$f_{\underline{P}}\left(\underline{p}\right) = \int_{\{\underline{u}: R_t(\underline{u}) + R_o(\underline{u}) = n_a\}} f_{\underline{P}|\underline{U}}\left(\underline{p}|\underline{u}\right) f_{\underline{U}}(\underline{u}) d\underline{u}$$

$$= \sum_{(r_t, r_o): r_t + r_o = n_a} \sum_{\{\mathbb{I} \subset [n_a]: |\mathbb{I}| = r_t\}} \frac{\lambda_t^{r_t} \lambda_o^{r_o}}{r_t! r_o!} e^{-A_t \lambda_t - A_o \lambda_o} \prod_{j \in \mathbb{I}} \mathcal{I}_{\mathcal{A}_t}(j) \prod_{j \in \mathbb{I}^c} \mathcal{I}_{\mathcal{A}_o}(j),$$

where the integral components are defined by

$$\mathcal{I}_{\mathcal{A}_\mathrm{t}}(j) = \int_{\mathcal{A}_\mathrm{t}} f_{\mathbf{P}_j|\mathbf{U}_j}(\mathbf{p}_j|\mathbf{u}_j)d\mathbf{u}_j \tag{3.5}$$

$$\mathcal{I}_{\mathcal{A}_\mathrm{o}}(j) = \int_{\mathcal{A}_\mathrm{o}} f_{\mathbf{P}_j|\mathbf{U}_j}(\mathbf{p}_j|\mathbf{u}_j)d\mathbf{u}_j. \tag{3.6}$$

Finally the posterior distribution of R_t, conditional on the gathered data is given by

$$\Pr\left(R_\mathrm{t} = r_\mathrm{t}|\underline{\mathbf{P}} = \underline{\mathbf{p}}\right)$$
$$= \sum_{\{\mathbb{I}\subset[n_\mathrm{a}]:|\mathbb{I}|=r_\mathrm{t}\}} \frac{\lambda_\mathrm{t}^{r_\mathrm{t}}\lambda_\mathrm{o}^{r_\mathrm{o}}e^{-A_\mathrm{t}\lambda_\mathrm{t}-A_\mathrm{o}\lambda_\mathrm{o}}}{r_\mathrm{t}!r_\mathrm{o}!f_{\underline{\mathbf{P}}}(\underline{\mathbf{p}})} \prod_{j\in\mathbb{I}}\mathcal{I}_{\mathcal{A}_\mathrm{t}}(j)\prod_{j\in\mathbb{I}^\mathrm{c}}\mathcal{I}_{\mathcal{A}_\mathrm{o}}(j).$$

Computing this conditional distribution of R_t given $\underline{\mathbf{P}}$ may appear difficult as it entails taking sums over subsets of $\{1, \ldots, n_\mathrm{a}\}$. However, by using generating functions, the posterior distribution can be calculated more efficiently [25].

The mean of the posterior distribution of R_t condition upon $\underline{\mathbf{P}}$ is the Bayes estimator,

$$\hat{R}_\mathrm{t}\left(\underline{\mathbf{p}}\right) = \mathrm{E}\left[R_\mathrm{t}|\underline{\mathbf{P}} = \underline{\mathbf{p}}\right] = \sum_{r_\mathrm{t}=0}^{n_\mathrm{a}} r_\mathrm{t}\Pr\left(R_\mathrm{t} = r_\mathrm{t}|\underline{\mathbf{P}} = \underline{\mathbf{p}}\right). \tag{3.7}$$

We adopt the Bayesian mean squared error (BMSE) to evaluate the performance of the estimator,

$$\mathrm{BMSE}\left[\hat{R}_\mathrm{t}\right] = \mathrm{E}\left[\left(\hat{R}_\mathrm{t}\left(\underline{\mathbf{P}}\right) - R_\mathrm{t}\right)^2\right]. \tag{3.8}$$

This BMSE can be approximated by taking the average over samples,

$$\mathrm{BMSE}\left[\hat{R}_\mathrm{t}\right] \approx \frac{1}{M}\sum_{m=1}^{M}\left(\hat{R}_\mathrm{t}^{(m)}\left(\underline{\mathbf{P}}^{(m)}\right) - R_\mathrm{t}^{(m)}\right)^2. \tag{3.9}$$

3.2 Maximum Likelihood Estimation

In this section, we assume the Poisson intensity parameters λ_t and λ_o are unavailable. For this scenario, we employ a classical approach and adopt maximum-likelihood estimation [26]. The distribution of $\underline{U}$ can be written as

$$f_{\underline{U}}\left(\underline{u}; \lambda_t, \lambda_o\right) = \frac{\lambda_t^{R_t(\underline{u})} \lambda_o^{R_o(\underline{u})}}{(R_t(\underline{u}))! \, (R_o(\underline{u}))!} e^{-A_t \lambda_t - A_o \lambda_o}. \tag{3.10}$$

The likelihood function is a function with two parameters, λ_t and λ_o

$$\mathcal{L}\left(\lambda_t, \lambda_o; \underline{p}, \underline{u}\right) = f_{\underline{P}, \underline{U}}\left(\underline{p}, \underline{u}; \lambda_t, \lambda_o\right) = f_{\underline{P}|\underline{U}}\left(\underline{p}|\underline{u}\right) f_{\underline{U}}\left(\underline{u}; \lambda_t, \lambda_o\right). \tag{3.11}$$

By computing the integral over $\underline{U}$, we can get the marginal likelihood function

$$\begin{aligned}
\mathcal{L}\left(\lambda_t, \lambda_o; \underline{p}\right) &= \int_{\{\underline{u}: R_t(\underline{u}) + R_o(\underline{u}) = n_a\}} f_{\underline{P}|\underline{U}}\left(\underline{p}|\underline{u}\right) f_{\underline{U}}\left(\underline{u}; \lambda_t, \lambda_o\right) d\underline{u} \\
&= e^{-A_t \lambda_t - A_o \lambda_o} \sum_{(r_t, r_o): r_t + r_o = n_a} \frac{\lambda_t^{r_t} \lambda_o^{r_o}}{r_t! r_o!} \sum_{\{\mathbb{I} \subset [n_a] : |\mathbb{I}| = r_t\}} \prod_{j \in \mathbb{I}} \mathcal{I}_{\mathcal{A}_t}(j) \prod_{j \in \mathbb{I}^c} \mathcal{I}_{\mathcal{A}_o}(j).
\end{aligned} \tag{3.12}$$

This results in a two-dimensional optimization for maximizing the likelihood. But, we can simplify it to a one-dimensional optimization problem by the following property,

$$\max_{\lambda_t, \lambda_o} \mathcal{L}\left(\lambda_t, \lambda_o; \underline{p}\right) = \max_{\alpha} \mathcal{L}\left(\frac{n_a}{A_t}\alpha, \frac{n_a}{A_o}(1-\alpha); \underline{p}\right) \tag{3.13}$$

where α within the interval $[0, 1]$. Under this property, we can rewrite the likelihood function in terms of α as

$$\mathcal{L}\left(\frac{n_{\mathrm{a}}}{A_{\mathrm{t}}}\alpha, \frac{n_{\mathrm{a}}}{A_{\mathrm{o}}}(1-\alpha); \underline{\mathbf{p}}\right)$$

$$= \sum_{(r_{\mathrm{t}},r_{\mathrm{o}}):r_{\mathrm{t}}+r_{\mathrm{o}}=n_{\mathrm{a}}} \frac{e^{-n_{\mathrm{a}}}n_{\mathrm{a}}^{n_{\mathrm{a}}}}{r_{\mathrm{t}}!r_{\mathrm{o}}!} \left(\frac{\alpha}{A_{\mathrm{t}}}\right)^{r_{\mathrm{t}}} \left(\frac{1-\alpha}{A_{\mathrm{o}}}\right)^{r_{\mathrm{o}}} \sum_{\{\mathbb{I}\subset[n_{\mathrm{a}}]:|\mathbb{I}|=r_{\mathrm{t}}\}} \prod_{j\in\mathbb{I}} \mathcal{I}_{\mathcal{A}_{\mathrm{t}}}(j) \prod_{j\in\mathbb{I}^{\mathrm{c}}} \mathcal{I}_{\mathcal{A}_{\mathrm{o}}}(j).$$

$$(3.14)$$

At this point, we can use standard numerical methods to get the values of λ_{t} and λ_{o} that maximize the likelihood function. Once λ_{t} and λ_{o} are obtained, the maximum likelihood estimator can be calculated as

$$\hat{R}_{\mathrm{t}}\left(\underline{\mathbf{p}}\right) = \mathrm{E}_{\hat{\lambda}_{\mathrm{t}},\hat{\lambda}_{\mathrm{o}}}\left[R_{\mathrm{t}}|\underline{\mathbf{P}} = \underline{\mathbf{p}}\right]$$

$$= \sum_{r_{\mathrm{t}}=0}^{n_{\mathrm{a}}} r_{\mathrm{t}} \Pr\left(R_{\mathrm{t}} = r_{\mathrm{t}}|\underline{\mathbf{P}} = \underline{\mathbf{p}}; \hat{\lambda}_{\mathrm{t}}, \hat{\lambda}_{\mathrm{o}}\right). \tag{3.15}$$

We adopt the mean squared error (MSE) to evaluate the performance of our estimator,

$$\mathrm{MSE}\left[\hat{R}_{\mathrm{t}}\right] = \mathrm{E}\left[\left(\hat{R}_{\mathrm{t}}\left(\underline{\mathbf{P}}\right) - R_{\mathrm{t}}\right)^2\right]. \tag{3.16}$$

This mean squared error can be approximated by taking the average over samples numerically,

$$\mathrm{MSE}\left[\hat{R}_{\mathrm{t}}\right] \approx \frac{1}{M}\sum_{m=1}^{M}\left(\hat{R}_{\mathrm{t}}^{(m)}\left(\underline{\mathbf{P}}^{(m)}\right) - R_{\mathrm{t}}^{(m)}\right)^2. \tag{3.17}$$

4.   NUMERICAL SIMULATION SETUP AND RESULTS

In this section, we introduce our simulation setup, including the directional antenna model, the parameters of the channel and how we generate RSSI samples. The simulation results will be shown after that. The simulation code is written in Python. In the simulation framework, the set up consists of four monitoring devices placed at the corners of the area of interest. All antennas attached to monitoring devices are pointing towards the center of the area of interest. The target area is considered to be a square of dimension 6 m Œ 6 m inscribed in a larger square of dimension 10 mŒ10 m. The two square areas share a same center point. Again, we use A_t to denote the target area, while A_o denotes its complement. We call the inside region the target area, and we refer to its complement as the outside region in the following text.

4.1   Antenna Characteristic

To analyze the effect of radiation characteristics of the sensing antennas on the estimation, isotropic antennas and directional antennas are considered. The antenna gain of the isotropic antennas are zero in all directions. For the directional antennas, we adopt the 3GPP antenna model in [27]. The directional antenna gains obey the following formula,

$$G_i(\phi_{ij}) = -\min\left\{12\left(\frac{\phi_{ij} - \theta_i}{\theta_{3\text{dB}}}\right)^2, G_{\text{floor}}\right\} - G_{\text{avg}}$$

where θ_i is the pointing direction of the antenna that is attached to monitoring device i. Parameter $\theta_{3\text{dB}}$ is the 3 dB beam-width of the radiation pattern. Variable G_{floor} is a nominal attenuation floor. And, $G_{average}$ is a normalization factor, which equal to the average gain over $\in (-180°, 180°]$,
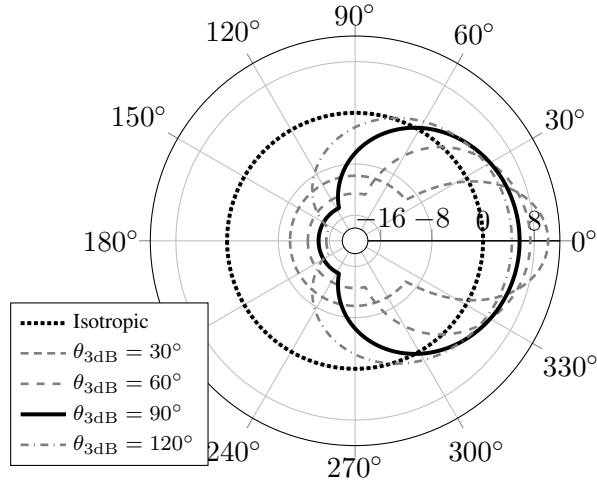
Figure 4.1: This graph depicts normalized antenna radiation patterns. The pointing direction is set to $0°$ and $G_{\text{floor}} = 20$ dB.

$$10 \log_{10} \left(\int_{-180}^{180} \frac{10^{-\frac{1}{10} \min\left\{ 12\left(\frac{\phi_{ij}-\theta_i}{\theta_{3\text{dB}}}\right)^2, G_{\text{floor}} \right\}}}{360} d\phi_{ij} \right).$$

The antenna radiation pattern for various 3 dB beam-widths is shown in Fig. 4.1.

4.2 Channel Characteristic

As mentioned in Section 2.1, the channel model we adopt is the log-normal path loss model. The received signal power can be expressed as

$$P[\text{dBm}] = A + B \log_{10}(d) + L + G(\phi). \tag{4.1}$$

In this equation, the physical parameters are based on regulation issued by the Federal Communications Commission (FCC) and on the profiles of typical wireless environments. According to the Friis transmission equation [28], we have

19

$$A = P_{\text{t}} + 20 \log_{10} \left(\frac{3 \times 10^8}{f_{\text{carrier}}} \right) - 20 \log_{10}(4\pi)$$

where P_t is the mobile devices transmission power, which is set to 20 dBm. The frequency $f_{carrier}$ is that of the Wi-Fi signal wave, 2.462 GHz [29]. Accordingly, A is equal to -20.27 dBm. We set the path-loss parameter B to -20 dBm, which is the coefficient associated with free-space. The logarithmic σ_s, which represents variation in shadow fading, is set to 2.0 dBm.

4.3   Generating Data Set

As mentioned above, the inference task is based on the received power matrix, which is collected by the monitoring devices. In the simulation, we generate the sample data according to the antenna gain model and the channel model discussed above. The parameter values we use to create the data set are summarized in Table 4.1.

Table 4.1: System parameters used during simulations.

Physical Parameters	Values
Nominal Power	$A = -20.27$ dBm
Free-Space Loss parameter	$B = -20$ dBm
Logarithmic Standard Deviation	$\sigma_{\text{s}} = 2.0$ dBm
3 dB Beam-width (directional)	$\theta_{\text{3dB}} = 90°$
Antenna Floor	$G_{\text{floor}} = 20$ dB

We generate the numerical data set as follows. We denote the location of the four monitoring devices as $\{\mathbf{s}_i\}$ where $i \in \{1, 2, 3, 4\}$. First, we set a certain value λ, which represents the aggregate Poisson rate across the two monitored regions (inside region and outside region) equal to 32. The splitting parameter between the two regions is α. Thus,

$$\lambda_{\mathrm{t}} = \alpha \frac{\lambda}{A_{\mathrm{t}}} \qquad\qquad \lambda_{\mathrm{o}} = (1 - \alpha)\frac{\lambda}{A_{\mathrm{o}}}$$

where λ_t is the Poisson rate of the inside region and λ_o is the Poisson rate of the outside region. Once λ_t and λ_o are determined, r_t the number of devices inside and r_o the number of devices outside are established using Poisson trials,

$$R_{\mathrm{t}} \sim \frac{(A_{\mathrm{t}}\lambda_{\mathrm{t}})^k}{k!}e^{-A_{\mathrm{t}}\lambda_{\mathrm{t}}} \qquad\qquad R_{\mathrm{o}} \sim \frac{(A_{\mathrm{o}}\lambda_{\mathrm{o}})^k}{k!}e^{-A_{\mathrm{o}}\lambda_{\mathrm{o}}}.$$

Each of the $R_t = r_t$ devices inside the target area is independently assigned a location according to a uniform distribution. Likewise, each of the $R_{\mathrm{o}} = r_{\mathrm{o}}$ devices outside is independently assigned a location according to another uniform distribution. Therefore, we obtain the location vector $\underline{\mathbf{U}} = \underline{\mathbf{u}}$ of the wireless clients. For each of the wireless clients, a collection of four received signal strength corresponding to the four monitoring devices is computed according to (4.1). The shadow fading component L is generated following a log-normal distribution whose standard deviation $\sigma_s = 2.0$ dBm. Finally, we get the sequence of power vectors $\underline{\mathbf{p}} = (\mathbf{p}_1, \ldots, \mathbf{p}_{n_{\mathrm{a}}})$, where vector $\mathbf{p}_j$ corresponding to wireless client j contains four power strength received by four monitoring devices, respectively.

4.4 Performance Analysis

The proposed estimators act on observation vector $\mathbf{p}$.

4.4.1 Bayes Estimation

We first consider the performance of the Bayes estimation framework introduced in Section 3.1. As is discussed in the previous section, the Poisson rate of the combined two regions λ, the Poisson rate of inside region λ_t and the Poisson rate of outside region λ_o have the following relation along with the splitting parameter α,

$$\lambda_{\mathrm{t}} = \alpha \frac{\lambda}{A_{\mathrm{t}}} \qquad\qquad \lambda_{\mathrm{o}} = (1 - \alpha)\frac{\lambda}{A_{\mathrm{o}}}.$$

In the simulation results, the area of the inside region A_t is equal to 36, and the area of the outside region A_o is equal to 64. We can plot performance results as a function of the splitting coefficient α. The vertical axis represents the BMSE of the Bayes estimator. The black curve in Fig. 4.2 shows the BMSE when the Bayes estimator operates on the data collected using isotropic antennas. The red curve in Fig. 4.2 corresponds to four directional antennas located at the four corners of the target area and pointing directly to the center. These antennas have a 3 dB beam-width of $\theta_{3\mathrm{dB}} = 90°$ and a nominal attenuation floor of $G_{\mathrm{floor}} = 20$ dB. Every point is obtained by averaging over fifty thousand trials.

According to Fig. 4.2, systems with directional antennas perform better than systems with isotropic antennas.

To further compare the performances, we introduce confidence intervals. A confidence level refers to the percentage of all possible samples that can be expected to include the true population parameter [30]. Suppose we use the same sampling method to select different samples and to compute a different interval estimate for each sample. Some interval estimates would include the true population parameter and some may not. A 95% confidence level means that 95% of the intervals would include the true parameter. Generally, the confidence interval is computed as below. Select a confidence level which describes
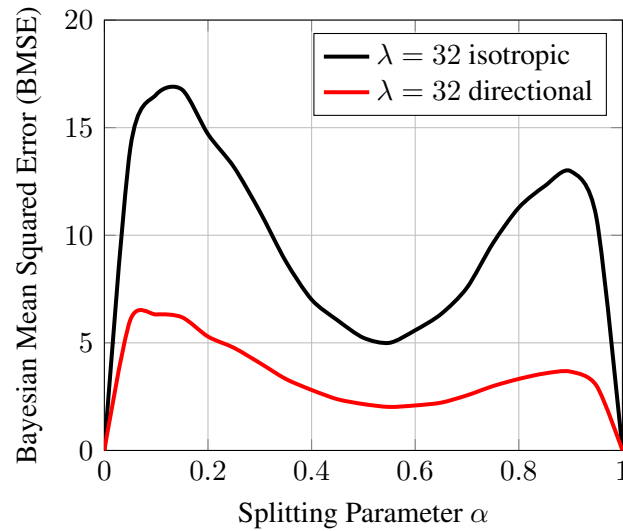
Figure 4.2: This graph shows the Bayesian mean squared error as functions of splitting parameter under the scheme of 3.1. The black line corresponds to the performance of the system equipped with isotropic antennas, whereas the red line corresponds to the performance of systems equipped with directional antennas.

the uncertainty of a sampling method. Compute

$$\gamma = 1 - (\text{confidence level}/100).$$

Find the critical probability p^*

$$p^* = 1 - \gamma/2.$$

Express the critical value as a t-statistic by using the degree of freedom and the critical probability, where the degree of freedom is equal to

$$df = N - 1$$

and N is the sample size. The standard error SE is given as

$$SE = \frac{\sigma}{\sqrt{N}}$$

where σ is the standard deviation of the sample. The margin of error is the product of the critical value t^* and SE. The confidence interval is expressed as

$$\text{Confidence interval} = \mu \pm \text{Margin of error}$$

where μ is the mean of the sample. In this simulation, we analyze the absolute difference between the true number of target devices r_t and the estimated result $\hat{r}_t$. The confidence intervals of $|r_t - \hat{r}_t|$ corresponding to isotropic antennas and directional antennas are summarized in Table 4.2. The result is based on fifty thousand samples.

Table 4.2: Confidence interval of $|r_t - \hat{r}_t|$ for the simulated Bayes scheme.

Antenna type	Confidence interval	Confidence level
Directional	1.412411 ± 0.002166	95%
Isotropic	2.454623 ± 0.003450	95%

To make the result more straightforward, we use a Gaussian kernel density estimation to plot the approximation of the probability density function of $|r_t - \hat{r}_t|$. The horizontal axis represents value for $|r_t - \hat{r}_t|$.

Comparing the PDF curves in Fig. 4.3 and Fig. 4.4, the distribution of the error occurs in system with directional antennas appears closer to zero. This result, along with fact that the BMSE of directional systems is smaller, shows that systems with directional antennas perform better. This performance improvement results from the directional antennas being more discriminating than the isotropic antennas.
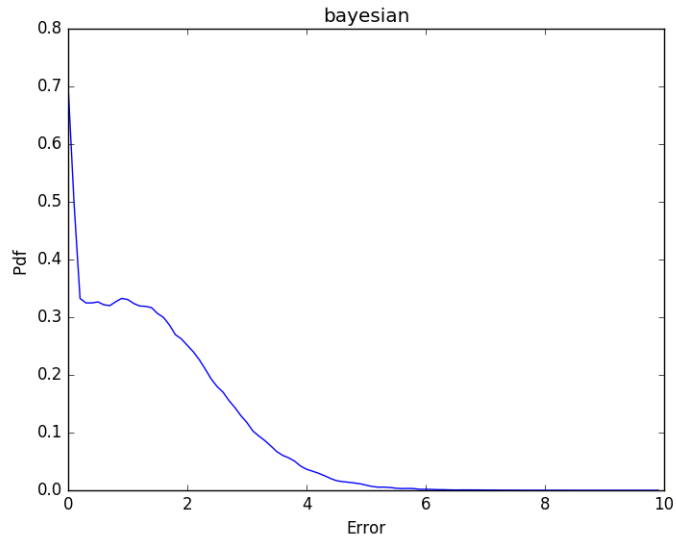
Figure 4.3: This graph shows the approximation probability density function of $|r_t - \hat{r}_t|$ corresponding to the system equipped with directional antennas under the scheme of Section 3.1.
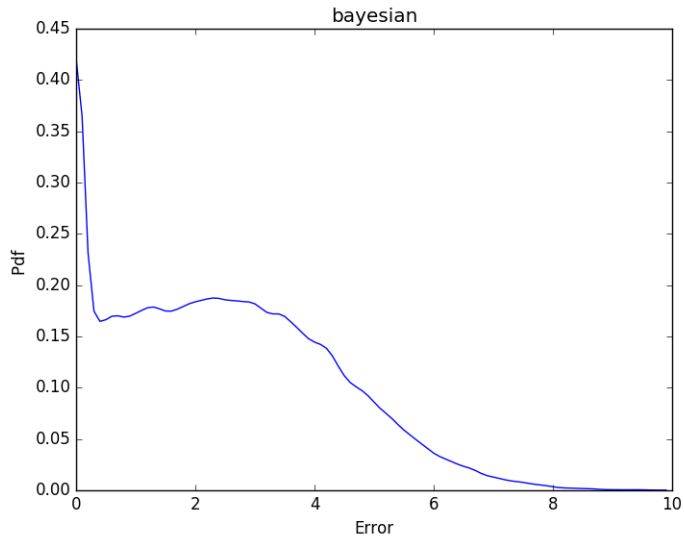

Figure 4.4: This graph shows the approximation probability density function of $|r_t - \hat{r}_t|$ corresponding to the system equipped with isotropic antennas under the scheme of Section 3.1.
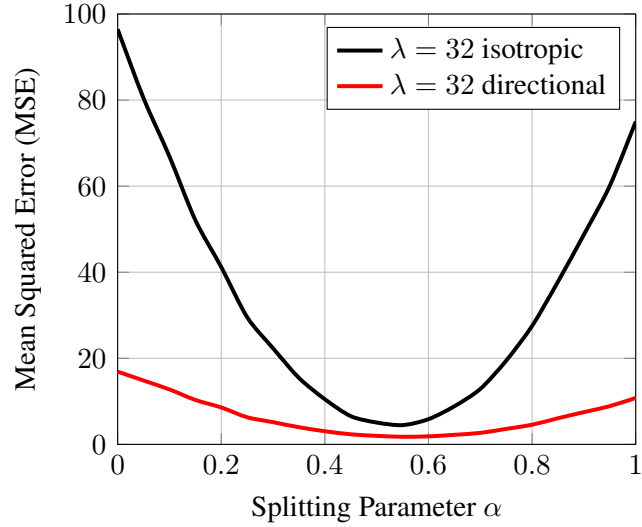
Figure 4.5: This figure shows the mean squared error as functions of splitting parameter under scheme of Section 3.2. The black line corresponds to the performance of a system equipped with isotropic antennas, whereas the red line corresponds to the performance of a system with directional antennas.

4.4.2 Maximum Likelihood Estimation

In this section, we look into the maximum likelihood estimation framework mentioned in Section 3.2. We use the average mean squared error to evaluate the performance of our estimator. As before, the total Poisson rates is set to be 32 and the curves are functions of splitting coefficient α.

The black curve in Fig. 4.5 shows the MSE when the maximum likelihood estimator operates on data collected using isotropic antennas. The red curve in Fig. 4.5 corresponds to the scenario where the estimator operates on data collected by directional antennas. The four directional antennas are located at the four corners of the target area, and they are pointing directly towards the center. These antennas have a 3 dB beam-width of $\theta_{3\text{dB}} = 90°$ and a nominal attenuation floor of $G_{\text{floor}} = 20$ dB. Every point is obtained by averaging over fifty thousand trials. The MSE is smaller for systems using directional antennas.
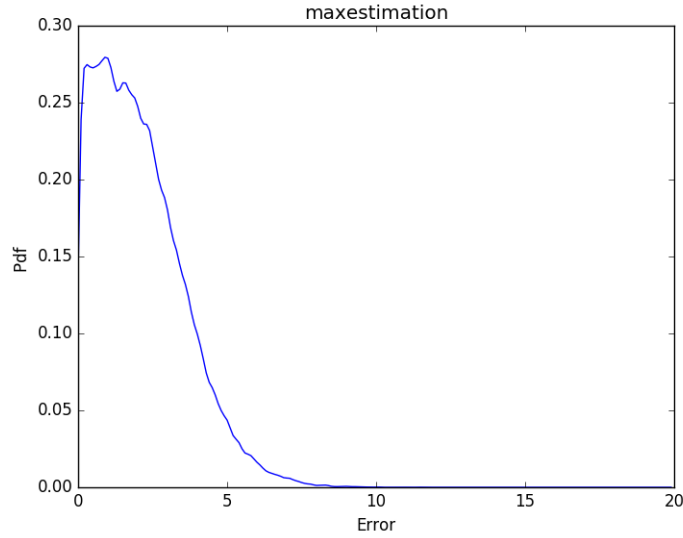
Figure 4.6: This graph shows the approximation probability density function of $|r_t - \hat{r}_t|$ corresponding to system equipped with directional antennas under scheme of 3.2.

The confidence interval of the absolute error $|r_t - \hat{r}_t|$ corresponding to the isotropic antennas and the directional antennas are summarized in Table 4.3.

Table 4.3: Confidence interval of $|r_t - \hat{r}_t|$ for simulation corresponding to the Maximum likelihood scheme.

Antenna type	Confidence interval	Confidence level
Directional	2.080484 ± 0.002809	95%
Isotropic	4.972427 ± 0.006020	95%

Comparing the PDF curves in Fig. 4.6 and Fig. 4.7, we see that the distribution of the error for systems with directional antennas appears closer to zero. This result, along with the fact that the MSE for the directional systems is smaller, shows that directional antennas outperform isotropic antennas within this context. Again, these results indicate that the information obtained from the directional antennas is more discriminating than the
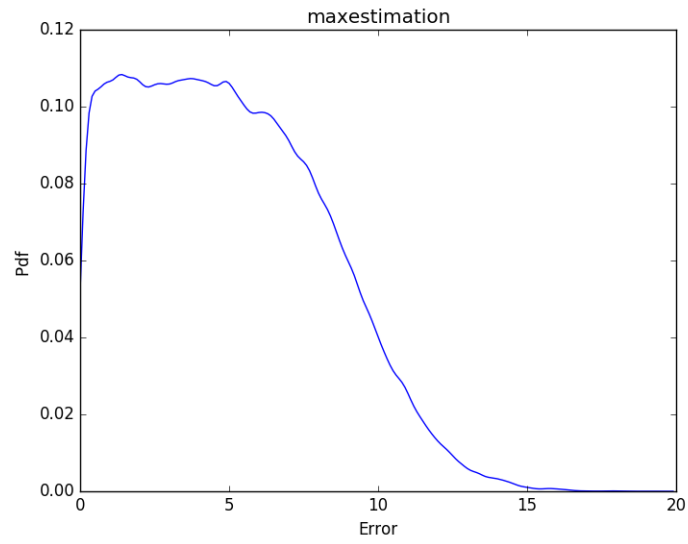
27

maxestimation

Figure 4.7: This graph shows the approximation probability density function of $|r_t - \hat{r_t}|$ corresponding to system equipped with isotropic antennas under scheme of 3.2.

that gathered by isotropic antennas.

5. EXPERIMENTAL IMPLEMENTATION

To complement the numerical findings based on our theoretical framework, we take an experimental implementation to assess the two schemes proposed in this thesis. The RSSI data set is collected during this experiment. This information is also used to provide statistical evidence for the wireless channel model adopted throughout. This model is used to determine the characteristics of the environment. The system is designed to work on the 2.4 GHz ISM radio band, which is used by Wi-Fi technology. In this experiment, all the wireless clients are connected to a wireless access point. This section details the way the experimental components are designed, and it explains the analysis of the gathered information.

5.1 Monitoring Devices

Every sensing device takes the form of a Next Unit of Computing (NUC) by Intel™, and runs the Ubuntu 14.04 (GNU/Linux) operating system. Wireless monitoring is enabled through an Alfa™ `AWUS036NHA` wireless interface with a detachable antenna. The Atheros™ chipset is able to listen to transmission packets on a channel if monitoring mode is turned on. The sub-miniature version A (SMA) antenna connectors are used to attach either isotropic antennas or directional antennas. Each monitoring device is equipped with one directional antenna and one isotropic antenna. Wooden sticks are also employed to fix the two antennas attached to a monitoring devices, and they are positioned at different heights to reduce the interactions and the coupling effect between the two antennas. The radiation pattern of the directional antenna is shown in Fig. 5.1.

A sniffing software built on the `pcap` application programming interface captures and filters wireless packets. For filtering, we employ a hash table for removing the duplicates in the detected MAC addresses. The software creates a local database to store the MAC
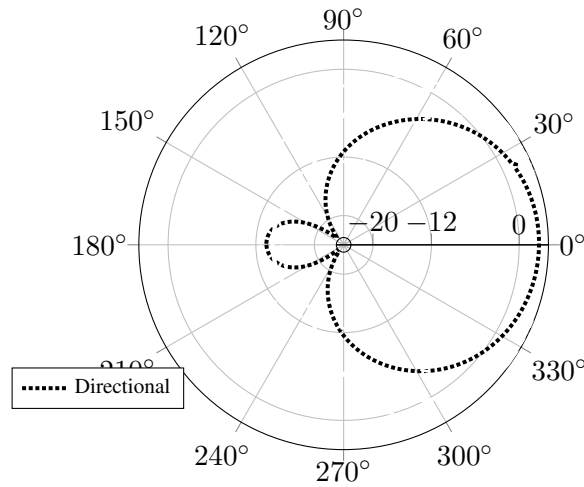
29

Figure 5.1: This graph depicts the directional antenna radiation pattern.

addresses and the RSSI values extracted from the wireless packets observed by the system. Finally the local database is sent to a central server for processing. The monitoring device we used during experiment is shown in Fig. 5.2.

5.2 Wireless Clients

In our experiment, the wireless clients are Android™ smartphones. All the wireless clients connect to a same local access point and send packets periodically, which makes them detectable by monitoring software. For the purpose of evaluating the performance of our estimators, not only do we need RSSI values, but we also need a ground truth (i.e., the true locations of the wireless clients). To this end, we employ a custom app that logs GPS coordinates and time. Throughout the experiment, the wireless clients periodically transmit the GPS information collected by their app to a central server. MAC addresses and time stamps are subsequently employed to match locations to power vectors at the center server, yielding a data set for performance evaluation.

Figure 5.2: This picture shows a custom monitoring device used in this experiment.

5.3 Experimental Samples

The experimental samples are divided into two categories: one is for monitoring devices with isotropic antennas, the other is for monitoring devices with directional antennas. Each category contains about 400 power and location vectors. Each power vector is in this form, $\underline{\mathbf{p}} = (\mathbf{p}_1, \ldots, \mathbf{p}_4)$, where $\mathbf{p}_i$ is the power received by monitoring device i. Since there are four monitoring devices, we have almost 3200 distinct data points.

Experimental trials are then conducted as follows. First we generate r_t the number of clients inside and r_o the number of clients outside according to Poisson process.

$$\lambda_t = \alpha \frac{\lambda}{A_t} \qquad\qquad \lambda_o = (1 - \alpha) \frac{\lambda}{A_o}.$$

Then, r_t entries are selected uniformly from clients in $\mathcal{A}_t$, and r_o entries are selected uniformly from clients in $\mathcal{A}_o$. The two collections of entries are combined into a single vector $\underline{p}$, which acts as input to the estimator. At last, the estimates are compared to the ground truth.

5.4 Channel Parameters

Channel parameters A and B can vary depending on the wireless environment. This experiment is conducted on widely open parking lot. Figure offers a satellite image view of the experiment site. The parameters are obtained by using the least squares method mentioned in Section 2.1. The parameters for the the isotropic systems are $A = -41.68$, $B = -16.07$ and $\sigma_s = 7.91$ dBm. Similarly, the parameters for the systems with directional antennas are $A = -34.72$, $B = -17.11$ and $\sigma_s = 8.31$ dBm.

5.5 Experiment Results

5.5.1 Performance of Bayes Estimation

The experimental results for the Bayes estimation scheme are shown in Fig. 5.4. The horizontal axis represents the splitting parameter α. The vertical axis corresponds to the BMSE. Each point is averaged over 10,000 trials.

The confidence intervals of $|r_t - \hat{r}_t|$ corresponding to isotropic antennas and directional antennas are summarized in Table 5.1.

Table 5.1: Confidence interval corresponding to $|r_t - \hat{r}_t|$ for the experimental Bayes scheme.

Antenna type	Confidence interval	Confidence level
Directional	3.317535 ± 0.010430	95%
Isotropic	3.331094 ± 0.010274	95%

Figure 5.3: This figure highlights the site used for the experiments, and it marks the locations of the mobile agents.
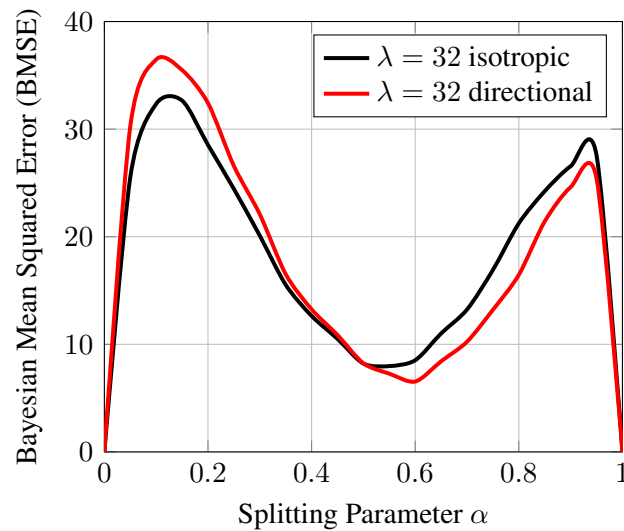

Figure 5.4: This figure depicts the experimental Bayesian mean squared error as a function of Poisson splitting coefficient α. The red line represents systems with directional antennas, whereas the black line represents system with isotropic antennas.
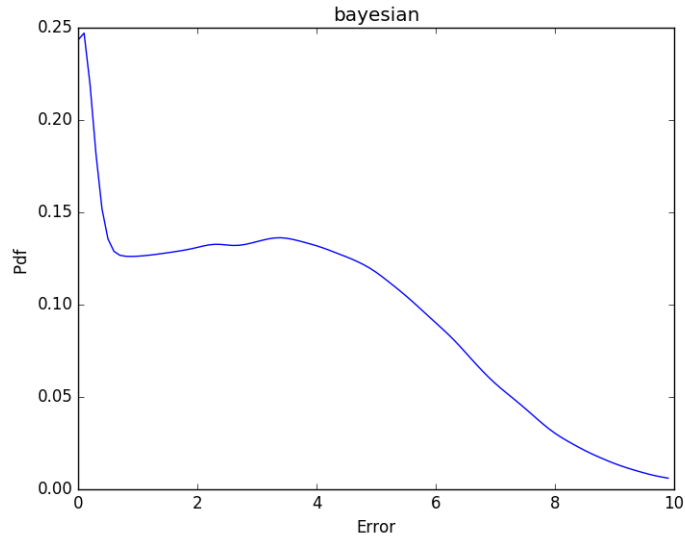
Figure 5.5: This graph shows the approximate probability density function for $|r_t - \hat{r}_t|$ corresponding to a system equipped with directional antennas under the scheme of Section 3.1.

The approximate probability density functions corresponding to systems with directional antennas and isotropic antennas are shown in Fig. 5.5 and Fig. 5.6.

In this case, using directional antennas does not bring an obvious benefit. The BMSE of the systems with directional antennas and that of the systems with isotropic antennas are very close. This phenomena may be caused by the inaccuracy of the GPS information. Small location errors may bring large estimation errors, especially when using directional antennas.

5.5.2 Performance of Maximum Likelihood Estimation

Experimental curves for the Bayes estimation scheme are shown in Fig. 5.7. The horizontal axis corresponds to the splitting parameter α. The vertical axis is the BMSE. Each point is obtained by averaging over 10,000 trials.

The confidence intervals of $|r_t - \hat{r}_t|$ corresponding to the isotropic antennas and direc-
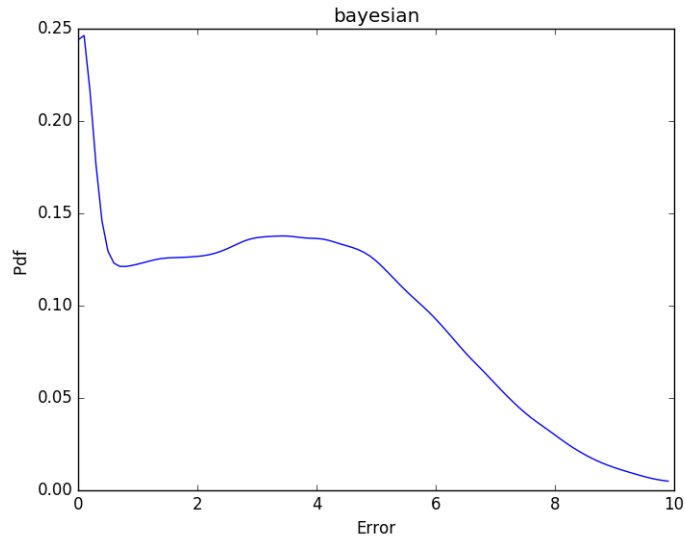
Figure 5.6: This graph shows the approximate probability density function for $|r_t - \hat{r}_t|$ corresponding to a system equipped with isotropic antennas under the scheme of Section 3.1.

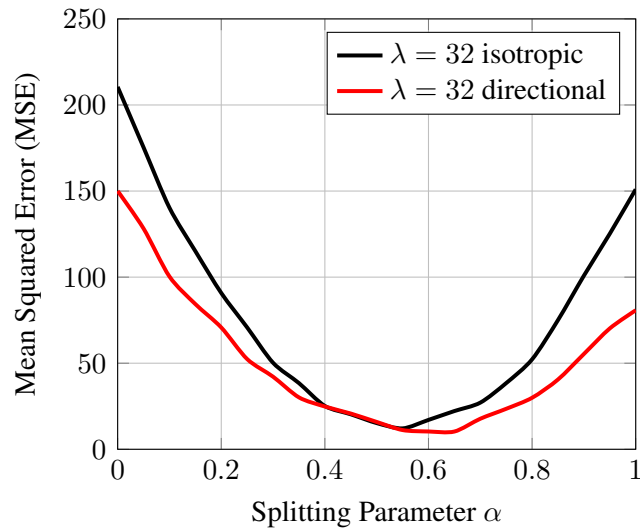Figure 5.7: This figure depicts the experimental Bayesian mean squared error as a function of Poisson splitting coefficient α. The red line represents systems with directional antennas, whereas the black line represents systems with isotropic antennas.
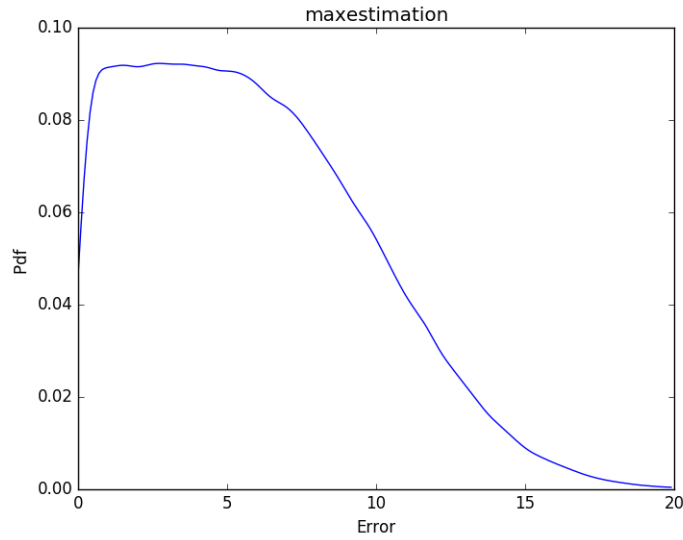
Figure 5.8: This graph shows the approximate probability density function of $|r_t - \hat{r}_t|$ corresponding to systems equipped with directional antennas under the scheme of Section 3.2.

tional antennas are summarized in Table 5.2.

Table 5.2: Confidence interval associated with $|r_t - \hat{r}_t|$ for the experimental maximum likelihood estimation scheme.

Antenna type	Confidence interval	Confidence level
Directional	5.881027 ± 0.016484	95%
Isotropic	7.144900 ± 0.019182	95%

The approximate probability density functions corresponding to systems with directional antennas and isotropic antennas are shown in Fig. 5.8 and Fig. 5.9.

In this case, the systems with directional antennas perform better, which implies that directional antennas are collectively more discrimination.
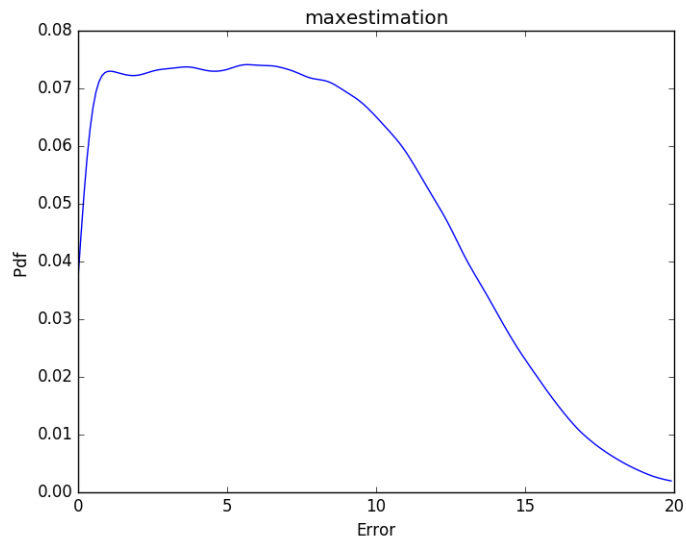
36

Figure 5.9: This graph shows the approximate probability density function of $|r_t - \hat{r}_t|$ corresponding to systems equipped with isotropic antennas under the scheme of Section 3.2.

6. CONCLUSION

In this thesis, we report two algorithms corresponding to different application scenarios for occupancy estimation using Wi-Fi monitoring. We utilize NUCs with sensing antennas as monitoring devices. We assess the performance of the estimators for isotropic and directional antennas through numerical simulations and prototyping. Our results indicate that it is possible to accurately estimate the number of active agents within a prescribed area by deploying sensing devices about the area of interest. Furthermore, performance is generally enhanced by the careful shaping of antenna radiation patterns. That is, the performance of a monitoring system can be enhanced by employing a configuration that strongly discriminates between wireless agents that are located within and outside the target area. In general, a more discriminating configuration yields considerable improvements over a generic setup with isotropic antennas.

This work can be extended for future research. Potential problems include tracking occupancy over time, and estimate the density of people using non-uniform distributions. It would also be interesting to use reconfigurable antennas to acquire very discriminating information about active devices for wireless inference. Finally, a pragmatic goal would be to implement such a monitoring system indoors, where multipath fading exists and tracking the location of a particular device can be very challenging. This information could then be used to dynamically adapt Wi-Fi access points to changing network traffic conditions.

REFERENCES

[1] T. A. Nguyen and M. Aiello, "Energy intelligent buildings based on user activity: A survey," *Energy and Buildings*, vol. 56, pp. 244 – 257, 2013.

[2] B. Balaji, J. Xu, A. Nwokafor, R. Gupta, and Y. Agarwal, "Sentinel: Occupancy based hvac actuation using existing wifi infrastructure within commercial buildings," in *Proceedings of the 11th ACM Conference on Embedded Networked Sensor Systems*, SenSys '13, (New York, NY, USA), pp. 17:1–17:14, ACM, 2013.

[3] D. Valerio, A. D'Alconzo, F. Ricciato, and W. Wiedermann, "Exploiting cellular networks for road traffic estimation: A survey and a research roadmap," in *Vehicular Technology Conference, 2009. VTC Spring 2009. IEEE 69th*, pp. 1–5, April 2009.

[4] Cisco Systems, Inc., *Visual Networking Index: Global Mobile Data Traffic Forecast Update*, 2016.

[5] C. Xu, B. Firner, R. S. Moore, Y. Zhang, W. Trappe, R. Howard, F. Zhang, and N. An, "Scpl: Indoor device-free multi-subject counting and localization using radio signal strength," in *Proceedings of the 12th International Conference on Information Processing in Sensor Networks*, IPSN '13, (New York, NY, USA), pp. 79–90, ACM, 2013.

[6] M. Seifeldin, A. Saeed, A. E. Kosba, A. El-Keyi, and M. Youssef, "Nuzzer: A large-scale device-free passive localization system for wireless environments," *IEEE Transactions on Mobile Computing*, vol. 12, pp. 1321–1334, July 2013.

[7] eMarketer, Inc., *Worldwide Internet and Mobile Users: eMarketers Updated Estimates for 2015*, 2015.

[8] comScore, *comScore Reports December 2015 U.S. Smartphone Subscriber Market Share*, 2015.

[9] T. S. Rappaport *et al.*, *Wireless communications: principles and practice*, vol. 2. Prentice Hall PTR New Jersey, 1996.

[10] H. L. Bertoni, *Radio propagation for modern wireless systems*. Pearson Education, 1999.

[11] G. L. Stüber, *Principles of mobile communication*. Springer Science & Business Media, 2011.

[12] Z. Ma and A. B. Chan, "Crossing the line: Crowd counting by integer programming with local features," in *The IEEE Conference on Computer Vision and Pattern Recognition (CVPR)*, June 2013.

[13] Y. Taniguchi, M. Mizushima, G. Hasegawa, H. Nakano, and M. Matsuoka, "Counting pedestrians passing through a line in crowded scenes by extracting optical flows," *International Information Institute (Tokyo).Information*, vol. 19, pp. 303–316, 01 2016. Copyright - Copyright International Information Institute Jan 2016; Document feature - Illustrations; Equations; Tables; Graphs; ; Last updated - 2016-07-30.

[14] M. Li, Z. Zhang, K. Huang, and T. Tan, "Estimating the number of people in crowded scenes by mid based foreground segmentation and head-shoulder detection," in *Pattern Recognition, 2008. ICPR 2008. 19th International Conference on*, pp. 1–4, IEEE, 2008.

[15] V. Garg and N. Bansal, "Smart occupancy sensors to reduce energy consumption," *Energy and Buildings*, vol. 32, no. 1, pp. 81 – 87, 2000.

[16] O. Shih and A. Rowe, "Occupancy estimation using ultrasonic chirps," in *Proceedings of the ACM/IEEE Sixth International Conference on Cyber-Physical Systems*,

ICCPS '15, (New York, NY, USA), pp. 149–158, ACM, 2015.

[17] Nishide, R., and H. Takada, "Exploring efficient methods to extract pedestrian flows on a mobile adhoc network," *The 6th International Conference on Mobile Ubiquitous Computing, Systems, Services and Technologies*, 2012.

[18] Depatla, Saandeep, Arjun Muralidharan, and Yasamin Mostofi, "Occupancy estimation using only wifi power measurements," *IEEE Journal on Selected Areas in Communications*, vol. 33, pp. 1381–1393, 05 2015.

[19] N. Abedi, A. Bhaskar, and E. Chung, "Bluetooth and wi-fi mac address based crowd data collection and monitoring : benefits, challenges and enhancement," in *36th Australasian Transport Research Forum (ATRF)*, (Queensland University of Technology, Brisbane, QLD), October 2013.

[20] W. Xi, J. Zhao, X. Y. Li, K. Zhao, S. Tang, X. Liu, and Z. Jiang, "Electronic frog eye: Counting crowd using wifi," in *IEEE INFOCOM 2014 - IEEE Conference on Computer Communications*, pp. 361–369, April 2014.

[21] S. Depatla, A. Muralidharan, and Y. Mostofi, "Occupancy estimation using only wifi power measurements," *IEEE Journal on Selected Areas in Communications*, vol. 33, pp. 1381–1393, July 2015.

[22] D. Zwillinger, *CRC standard mathematical tables and formulae*. CRC press, 2002.

[23] S. M. Kay, *Fundamentals of Statistical Signal Processing: Practical Algorithm Development*, vol. 3. Pearson Education, 2013.

[24] H. V. Poor, *An introduction to signal detection and estimation*. Springer Science & Business Media, 2013.

[25] R. L. Graham, D. E. Knuth, and O. Patashnik, *Concrete Mathematics: A Foundation for Computer Science*. Addison-Wesley, 2 edition ed., 1994.

[26] G. Casella and R. L. Berger, *Statistical Inference*. Duxbury Thomson Learning, 2nd edition ed., 2001.

[27] Technical Specification Group Radio Access Network, 3rd Generation Partnership Project, *Spatial Channel Model for Multiple Input Multiple Output (MIMO) Simulations*, 2011. release 10.

[28] H. T. Friis, "A note on a simple transmission formula," *Proceedings of the IRE*, vol. 34, no. 5, pp. 254–256, 1946.

[29] A. Goldsmith, *Wireless Communications*. Cambridge University Press, 2005.

[30] D. Altman, D. Machin, T. Bryant, and M. Gardner, *Statistics with confidence: confidence intervals and statistical guidelines*. John Wiley & Sons, 2013.